Effect of different degrees of adenoid hypertrophy on pediatric upper airway aerodynamics: a computational fluid dynamics study

Effect of different degrees of adenoid hypertrophy on pediatric upper airway aerodynamics: a computational fluid dynamics study

Zhenzhen Hu[1] · Jingliang Dong[2] · Miao Lou[1] · Jingbin Zhang[3] · Ruiping Ma[1] · Yusheng Wang[1] · Minjie Gong[1] · Botao Wang[1] · Zhenbo Tong[4] · Hongxian Ren[4] · Guoxi Zheng[1] · Ya Zhang[1]

[1] Department of Otolaryngology Head and Neck Surgery, The Second Affiliated Hospital of Xi'an Jiaotong University, Xi'an, Shaanxi, China

[2] Institute for Sustainable Industries & Liveable Cities, Victoria University, PO Box 14428, Melbourne, VIC, 8001, Australia

[3] Department of Imaging, The Second Affiliated Hospital of Xi'an Jiaotong University, Xi'an, Shaanxi, China

[4] School of Energy and Environment, Southeast University, Nanjing, China

The corresponding authors are Guoxi Zheng and Ya Zhang.

E-mail addresses: zhengguoxi888@sina.com (G. Zheng), zhangya@xjtu.edu.cn (Y. Zhang).

Corresponding authors at: 157 Xiwu Road, Xi 'an, Shaanxi, 710004, China.

Effect of different degrees of adenoid hypertrophy on pediatric upper airway aerodynamics: a computational fluid dynamics study

Abstract

To improve the diagnostic accuracy of adenoid hypertrophy (AH) in children and prevent further complications in time, it is important to study and quantify the effects of different degrees of AH on pediatric upper airway (UA) aerodynamics. In this study, based on computed tomography (CT) scans of a child with AH, UA models with different degrees of obstruction (adenoidal-nasopharyngeal (AN) ratio of 0.9, 0.8, 0.7, and 0.6) and no obstruction (AN ratio of 0.5) were constructed through virtual surgery to quantitatively analyze the aerodynamic characteristics of UA with different degrees of obstruction in terms of the peak velocity, pressure drop (ΔP), and maximum wall shear stress (WSS). We found that two obvious whirlpools are formed in the anterior upper part of the pediatric nasal cavity and in the oropharynx, which is caused by the sudden increase in the nasal cross-section area, resulting in local flow separation and counterflow. In addition, when the AN ratio was ≥ 0.7, the airflow velocity peaked at the protruding area in the nasopharynx, with an increase 1.1 to 2.7 times greater than that in the nasal valve area; the ΔP in the nasopharynx was significantly increased, with an increase 1.1-6.8 times greater than that in the nasal cavity; and the maximum WSS of the posterior wall of the nasopharynx was 1.1-4.4 times larger than that of the nasal cavity. The results showed that the size of the adenoid plays an important role in the patency of the pediatric UA.

Keywords Virtual surgery · Adenoid hypertrophy · AN ratio · CFD · Aerodynamics

1 Introduction

The adenoids, also known as the "nasopharyngeal tonsils", are normal lymphatic tissues at the roof of the nasopharynx that play a protective role in upper respiratory diseases (van Cauwenberge et al. 1995). Since Hans Wilhelm Meyer introduced the term adenoid hypertrophy (AH) in 1868, the diagnosis of AH has increased rapidly (Weir 1990). A recent meta-analysis showed that the prevalence of AH in children and adolescents was 34.46% (Pereira et al. 2018). Recurrent or chronic upper airway (UA) infections, allergic inflammation, and immune responses may lead to AH (Brambilla et al. 2014; Pagella et al. 2015). The presence of AH can cause mouth breathing, snoring, obstructive sleep apnea-hypopnea syndrome and, in some children, adenoid facies. Therefore, timely identification of airflow alterations caused by AH can help prevent further complications.

Currently, nasal endoscopy is considered the standard for clinically assessing the size of the adenoids in cooperative children (Bitar et al. 2009; Kubba and Bingham 2001; Kindermann et al. 2008). In addition, lateral cephalogram and cone beam computed tomography (CBCT) are also commonly used to evaluate the size, shape and position of adenoids in children, and the results show excellent consistency with those of nasal endoscopy (Duan et al. 2019; Pacheco-Pereira et al. 2016; Major et al. 2014). Assessment of adenoid size was an important part of the airflow change analysis in children's UA in this study. Adenoid size and the patency of the nasopharyngeal airway could be expressed by the adenoidal-nasopharyngeal (AN) ratio (Lertsburapa et al. 2010; Acar et al. 2014), which had been found to be significantly correlated with

nasopharyngeal volume (Feng et al. 2015). According to the AN ratio, Adedeji et al. (2016) classified the degree of obstruction of the nasopharyngeal airway by the adenoids as mild (0.60-0.69), moderate (0.70-0.79) and severe (0.80-0.89). Although many studies to date have established a relationship between the AN ratio and AH, the ultimate effect of different degrees of AH on respiratory function in terms of airflow alteration is still unclear.

Significant progress in computational fluid dynamics (CFD) has been made during the past two decades, and CFD has been widely used to predict the dynamic characteristics of target airflows because it allows the accurate and noninvasive quantitative analysis of air flow. At present, numerical research has been carried out on many aspects of nasal airflow, including nasal physiology (Horschler et al. 2003; Wen et al. 2008; Xu et al. 2020), nasal anatomical structure abnormalities (Li et al. 2016; Garcia et al. 2010), performance prediction of turbinectomy (Siu et al. 2021; Lee et al. 2016), and particle deposition (Wang et al. 2009; Siu et al. 2020; Zhang et al. 2019; Bahmanzadeh et al. 2015; Dong et al. 2018; Dong et al. 2017), which have greatly promoted precision medicine. However, most previous studies have focused on adult subjects, while nasal airflow in children has been less studied. Recently, Sun et al. (2022) studied the transport and deposition of nanoparticles in the nasal cavity of a 3-year-old child with AH. For children with AH, clinicians are still unable to quantify the relationship between adenoid morphology and the airflow characteristics of UA, which inevitably results in a degree of uncertainty with respect to diagnostic and treatment decision-making.

As a response to this research need, this paper presents a numerical study using an anatomically accurate pediatric UA model. Our research efforts are focused on the aerodynamic changes due to the presence of different degrees of AH. The research findings are expected to provide a scientific basis for helping treating physicians improve their diagnostic accuracy for AH in children and develop patient-specific treatment programs.

2 Materials and Methods

2.1 Data collection

CT scans of a 3-year-old child with AH were collected retrospectively. The CT scans included coronal, axial and sagittal images with a resolution of 512×512 pixels and a slice interval of 0.5 mm, covering the UA region. CT images were obtained in Digital Imaging and Communications in Medicine (DICOM) format. The nasal anatomy and morphology of the child showed no obvious abnormalities, and there was no history of serious maxillofacial abnormalities, sinusitis, nasal septum deviation, nasal tumors or nasal surgery. The parents provided written informed consent, and the study was approved by the institutional review board and the medical ethics committee of the Second Affiliated Hospital of Xi'an Jiaotong University (2020-819).

2.2 AN ratio measurement

The measurement method is shown in Fig. 1. Line BB is drawn along the straight part of the anterior margin of the basiocciput. The perpendicular distance from the outermost point of convexity of the adenoid shadow to BB is line segment AC, which represents the thickness of the adenoid. The distance from the posterior end of the hard

palate or the superior edge of the anterior middle area of the soft palate to the anteroinferior edge of the sphenooccipital synchondrosis is the line segment NC, which represents the width of the nasopharynx. The AN ratio is defined as the ratio of the thickness of the adenoid to the nasopharyngeal width, which reflects the adenoid size and nasopharyngeal airway patency (Fujioka et al. 1979).

2.3 3D reconstruction and CFD simulation

First, DICOM images were imported into the open-source software 3D-Slicer to reconstruct the UA. Paranasal sinuses were not included in the reconstruction because previous studies have indicated that they only have a minimal impact on intranasal airflow (Hood et al. 2009; Xiong et al. 2008; Ge et al. 2012). The geometry of the face was retained, and a hemisphere with a diameter of 100 mm was attached in front of the face. To investigate the influence of different levels of AH on pediatric UA aerodynamics, UA models with different degrees of obstruction (AN ratio of 0.9, 0.8, 0.7, and 0.6) and no obstruction (AN ratio of 0.5) were achieved by adjusting the extent of segmentation for the adenoid region (Fig. 2). The rest of the constructed model was consistent with the original CT images except for the nasopharynx, where virtual surgery was performed.

After model construction, the model was imported into Geomagic Studio 2015 (Geomagic, North Carolina, USA) for surface smoothing and regional division. The model was then exported in stereolithography (STL) format. ICEM-CFD 2021 R1 (ANSYS, Inc., Canonsburg, Pennsylvania) was used for tetrahedral and boundary layer meshing and 3D computational domain generation. Models with 1.6, 3.1, and 6.3

million grids were selected for the grid independence test on a representative line. The representative line started from the left nasal vestibule and ended at the nasopharynx along the y-axis (Fig. 3A). As the grid number increased from 3.1 million to 6.3 million, the average velocity change was less than 1% (Fig. 3B). The models used for simulation in this study had 5434816, 5506198, 5564851, 5623245, and 5690966 grids, respectively (Table 1).

The tidal volume and respiratory rate of three-year-old children were obtained according to the respiratory parameters published in the literature (Hofmann 1982), and the calculated inspiratory flow rate was 8.7 L/min, which is consistent with the setting reported by Xi et al. (2014). Besides, children's nasal cavities possess a complex structure and are significantly smaller than those of adults. In airflow limiting regions, such as the nasal vestibule and nasopharyngeal region, the airflow accelerates to become transitional and turbulent flow due to the significantly narrowed passage space (Doorly et al. 2008). Therefore, the SST κ-ω model was used to account for laminar and transitional flow regimes in the entire airway section in this paper, which is consistent with the setting of the study by Feng et al. (2021) on children. As the quasi-steady airflow assumption in the nasal cavity was found to be reasonable in previous studies (Yan et al.2023), thus the present study treated nasal airflows as quasi-steady flow, and the incompressible Navier-Stokes equation was used as the flow governing equation. The boundary conditions were set as follows: (1) the airway wall was assumed to be no-slip (zero velocity) and rigid; (2) the hemisphere in front of the face was defined as the "pressure inlet" with zero gauge pressure; and (3) the outlet of the

pharynx was defined as the "velocity outlet", and the velocity magnitude was calculated by dividing the volumetric flow rate by the outlet area.

Finally, CFD-POST 2021 R1 (ANSYS, Inc., Canonsburg, Pennsylvania) was used for post-processing. For better trans-airway flow analysis, five sections perpendicular to the main streamline were created in the UA (Fig. 4). The anterior nostril section was defined as C0, while C1 represented the section in the nasal valve area. C2 was the section of the choana, and the section at the narrowest part of the nasopharynx was C3. C4 was the section located at the free edge of the soft palate. The pressure drop in the nasal cavity refers to the pressure difference between C0 and C2, and the pressure drop in the nasopharynx refers to the pressure difference between C2 and C4. Through the above auxiliary sections, we analyzed changes in the airflow velocity, pressure drop ($\triangle P$) and wall shear stress (WSS).

3 Results

3.1 Model validation

An in vitro experimental system was designed and constructed for CFD validation (Fig. 5). The 1:1 scaled UA model was produced by the three-dimensional (3D) stereolithography (STL) technique using photosensitive resin material. Then, an artificial three-way airway was made and connected to the pharyngeal outlet of the model for nasal resistance testing. A flow probe was placed at the left nostril of the model, and the right nostril was sealed to detect the flow rates or velocity that being conducted by the left nasal chamber. A pressure probe was placed at the three-way opening of the throat to measure the transnasal pressure. The experimenter breathed

calmly through the PP nozzle of the three-way tube. The pressure drop between the left nostril and pharyngeal outlet was calculated by subtracting the pressure probe pressure from the environmental pressure (0 Pa).

A series of CFD simulations were correspondingly performed with the same airway geometry and boundary conditions as the experiments. The CFD results of pressure drop in the nasal models were compared with rhinomanometry (Equipment Model NR6, GM Instruments) measurements for different flow rates. Figure 6 shows pressure drop against air flow rate between numerical and experimental results plotted in the inspiration phase. The results showed a positive correlation between the pressure drop and flow rates for both experimental measurements and numerical simulations. As the inhalation flow rates increased from 5 L to 15 L, the pressure drop gradually increased from near 7.13 Pa to 51.16 Pa, and close agreement was achieved between numerical predictions and experimental data. Therefore, the CFD model is validated and can be used for further airflow analysis.

3.2 Geometric characteristics

When the AN ratio was adjusted from 0.9 to 0.5, the volume of the nasopharynx gradually increased. When the AN ratio was 0.9, the nasopharyngeal volume was the smallest (1380.68 mm^3), and when the AN ratio was 0.5, the nasopharyngeal volume was the largest (2857.81 mm^3). In models with an AN ratio of 0.9 to 0.5, the cross-sectional area of the nasopharynx at its narrowest point was 21.21 mm^2, 39.96 mm^2, 58.94 mm^2, 82.59 mm^2 and 110.61 mm^2, respectively. The above geometric information is listed in Table 1.

3.3 Airflow characteristics and velocity

When the AN ratio was 0.5, nasal airflow passed obliquely upward from the nostrils into the nasal cavity, and then the majority of the airflow was diverted horizontally backward after passing through the nasal valve. After exiting the choana, the direction of airflow again changes, as it is directed downward into the pharynx. The angles of the two changes in direction are approximately 45 degrees in both cases. There are significantly more airflow streamlines in the middle and inferior parts of the nasal cavity than in the superior part. Two obvious whirlpools are formed in the anterior upper part of the nasal cavity and in the oropharynx, which is caused by the sudden increase in the nasal cross-section area, resulting in local flow separation and counterflow. For children with AH, the turning angle of nasal airflow into pharynx increases with increasing AN ratio.

The high-velocity regions in the models were mainly located in the nasal valve and nasopharynx (Fig. 7). In the models with an AN ratio of 0.9 to 0.5, the maximum velocity decreased continuously with decreasing nasopharyngeal obstruction (maximum, 8.94 m/s; minimum, 2.28 m/s), and the mean velocity of the nasopharynx also decreased gradually (Fig. 8A). In the models with AN ratios of 0.9, 0.8 and 0.7, the airflow velocity peaked at the narrowest part of the nasopharynx, at 1.1 to 2.7 times that of the nasal valve area (8.94>3.34 m/s, 4.69>3.24 m/s, 3.45>3.25 m/s), while the peak velocity of the nasopharynx was less than that of the nasal valve in the models with AN ratios of 0.6 and 0.5 (2.67<3.25 m/s, 2.28<3.25 m/s) (Fig. 8B).

3.4 Pressure drop (ΔP)

223 The pressure changes were most significant at the nasal valve and nasopharynx
224 (Fig. 9); therefore, we analyzed the changes in nasal ΔP and nasopharyngeal ΔP. As the
225 AN ratio increased (from 0.5 to 0.9), the ΔP in the nasopharynx gradually increased
226 (maximum, 37.97 Pa; minimum, 5.00 Pa) (Fig. 10). For the models with AN ratios of
227 0.9, 0.8 and 0.7, the ΔP in the nasopharynx was significantly increased, with an increase
228 1.1 to 6.8 times greater than that in the nasal cavity (37.97>5.61 Pa, 9.90>5.65 Pa,
229 6.15>5.66 Pa), while for the models with AN ratios of 0.6 and 0.5, the nasopharyngeal
230 ΔP was significantly reduced and smaller than that of the nasal cavity (5.23<5.71 Pa,
231 5.00<5.73 Pa) (Fig. 10).

232 **3.5 Wall shear stress (WSS)**

233 The areas with the most obvious WSS changes were mainly in the nasal valve, the
234 anterior medial area of the middle turbinate and the posterior wall of the nasopharynx
235 (Fig. 11). With decreases in the AN ratio, the maximum WSS of the posterior wall of
236 the nasopharynx decreased continuously (maximum, 2.57 Pa; minimum, 0.33 Pa), and
237 the mean WSS of the posterior wall of the nasopharynx also decreased gradually (Fig.
238 12A). When the AN ratio was 0.9, 0.8, and 0.7, the maximum WSS of the posterior
239 wall of the nasopharynx was 1.1-4.4 times larger than that of the nasal cavity (2.57>0.58
240 Pa, 0.96>0.66 Pa, 0.77>0.67 Pa); however, when the AN ratio was 0.6 and 0.5, the
241 maximum WSS of the posterior wall of the nasopharynx was less than that of the nasal
242 cavity (0.45<0.67 Pa, 0.33<0.68 Pa) (Fig. 12B).

243 **3.6 Cross-sectional area and pressure drop and velocity**

244 With increases in the AN ratio, the cross-sectional area at the narrowest part of the

nasopharynx gradually decreased (Fig. 13A). The cross-sectional area of the nasal valve area was 74.77 mm^2. When the AN ratio was ≥0.7, the cross-sectional area of the nasal valve area was 1.3-3.5 times greater than that of the narrowest part of the nasopharynx (Fig. 13A). The maximum velocity and ΔP of the nasopharynx gradually increased with decreasing cross-sectional area of the narrowest part of the nasopharynx (Fig. 13B).

4 Discussion

With the improvement of computer technology, CFD has become widely used in the study of adult nasal aerodynamics. In this study, the morphology of the pediatric UA expressed as AN ratio was correlated with aerodynamic characteristics through CFD technology. We found that the airflow direction in a child's nasal cavity was the same as that in the adult nasal cavity (Wen et al. 2008; Lou et al. 2021), which helps to maintain the basic function of the nasal cavity in children. In children, a widespread area of the nasal cavity is in direct contact with the main airflow streamline, including its superior (partially), middle and inferior meatus regions. In adults, most airflow was diverted into the widest meatus of the nasal cavity - the middle meatus (Dong et al. 2022). This difference indicates a simple and immature nasal turbinate structure in children. In the UA models with an AN ratio of 0.5 to 0.9, the maximum velocity and pressure drop of the nasopharynx and the maximum WSS of the posterior wall of the nasopharynx varied significantly. This allowed the effect of the AN ratio on nasopharyngeal airflow dynamics to be quantified. Therefore, CFD technology may be an additional diagnostic tool for visualizing the airflow pattern in the UA and revealing aerodynamic characteristics.

Different degrees of AH lead to different degrees of nasopharyngeal airway obstruction, which leads to significant changes in the airflow characteristics of the UA. We found that the more severe the obstruction of the nasopharyngeal airway by adenoids, the greater the maximum velocity and pressure drop in the nasopharynx. This is because under the condition of a constant flow rate, with the increase in the AN ratio, the cross-sectional area at the narrowest part of the nasopharynx gradually decreases, resulting in a significant increase in the maximum velocity and pressure drop. This relationship between the morphology and aerodynamics of the UA in children can be explained by the Bernoulli effect (Weese et al. 2017), which states that when a fluid flows through a narrowing region of a tube, an increase in the speed of the fluid coincides with a decrease in pressure. In addition, the maximum WSS of the posterior wall of the nasopharynx increased gradually in the models with an AN ratio of 0.5 to 0.9. Structurally, the enlarged adenoids reduce the angle between the posterior wall of the nasopharynx and the plane of the choana, resulting in an increase in the impact force of nasal airflow on the posterior wall of the pharynx. Therefore, for children with AH, attention should also be given to lymphoid follicular hyperplasia in the posterior wall of the nasopharynx, and clinical intervention should be considered if necessary.

Our results suggest that the AN ratio can be used as an effective parameter to estimate airflow changes in the UA. When the AN ratio was ≥ 0.7, the maximum velocity and pressure drop of the nasopharynx were greater than those of the nasal cavity, and the maximum WSS of the posterior wall of the nasopharynx increased significantly. However, when the AN ratio was <0.7, the maximum velocity and

289 pressure drop of the nasopharynx and the maximum WSS of the posterior wall of the
290 nasopharynx were smaller than those of the nasal cavity. This indicates that an AN ratio
291 of 0.7 is the critical value leading to abnormal airflow dynamics. Xu et al. (2006)
292 conducted a study of children with OSAS and found that the pressure drop mainly
293 occurred between the choana and the region where the adenoids overlap the tonsils
294 (overlap region) due to airway narrowing, rather than in the nasal passages. The
295 findings of this study further suggest that this can occur when the AN ratio is ≥0.7. In
296 addition, the clinical symptoms of children with AH are significantly correlated with
297 the degree of nasopharyngeal airway obstruction determined by the AN ratio (Adedeji
298 et al. 2016). When the AN ratio was ≥0.7, the narrowest position of the UA was located
299 in the nasopharynx rather than the nasal valve, leading to an abnormal airway resistance
300 distribution. Children may show marked nasal obstruction, snoring, sleep apnea,
301 excessive daytime sleepiness and failure to thrive. For the model with mild
302 nasopharyngeal airway obstruction (AN ratio <0.7), the abnormal aerodynamics of the
303 UA disappeared, and the children's symptoms were relatively mild and easily ignored.
304 In clinical assessment, an AN ratio of >0.7 has been well accepted for indicating
305 pathological AH, and adenoidectomy may be suggested by clinicians (Elwany 1987;
306 Ungkanont and Damrongsak 2004). Our study provides a more comprehensive and
307 reliable aerodynamic basis for clinical evaluation and treatment. Luo et al. (2014) and
308 Mihaescu et al. (2008) found that after adenoidectomy and tonsillectomy, the
309 pharyngeal pressure drop in obese children with OSAS was significantly reduced. This
310 is mainly attributed to the increase in the volume of the pharyngeal cavity achieved by

surgery, which caused a decrease in pressure drop to relieve the patient's clinical symptoms.

This study reinforces the influence of the AN ratio on UA aerodynamics. The higher the AN ratio, the more severely the nasopharyngeal airway is obstructed by adenoids, which causes significant alterations in airflow dynamics. This change will seriously affect the growth and development of children and may lead to various complications, potentially impairing their quality of life. The results of this study preliminarily verify the feasibility of digital medical treatment for pediatric AH, which has potential as an effective tool for clinicians to preliminarily assess airflow changes caused by different degrees of AH and develop timely patient-specific treatment plans. The research method developed in this study can further be applied for the flow and inhalation exposure analysis in other respiratory disorders, such as laryngeal carcinoma (Beni et al. 2022). By virtually including the laryngeal tumour with different size, the effect of airway reduction can be assessed. Lastly, all these pre-operative evaluations are expected to assist relevant specialists in improving diagnosis accuracy and achieving optimal operation outcome.

There are some limitations to this study. 1. Due to the complexity of modeling and the need for CT scanning, only one child was analyzed. 2. Poor professional ability and computer skills may lead to inconsistent modeling results. 3. The models may be slightly different after surface segmentation and smoothing. 4. Future studies should consider the flexibility of the model wall and the fluid-solid interaction between the air and the respiratory tract wall (Beni et al. 2019; Beni et al. 2022).

5 Conclusions

When the AN ratio was ≥0.7, the narrowest position of the UA was located in the nasopharynx rather than the nasal valve, leading to an abnormal airway resistance distribution (nasopharyngeal pressure drop > nasal pressure drop). When the AN ratio was ≥0.7, the airflow velocity and WSS of the posterior wall of the nasopharynx increased significantly, acting as a potential aerodynamic factor for lymphoid follicular hyperplasia in this area. Therefore, CFD numerical simulation can provide objective and qualitative guidance for surgical planning of children with AH.

In conclusion, different degrees of AH can significantly affect the aerodynamic characteristics of the UA. For a UA with an AN ratio larger than 0.7, regions with AH dominated the nasopharyngeal flow field with a significant flow-limiting effect. Predicted aerodynamic parameters can assist relevant professionals in performing accurate diagnostic assessments and formulating individualized treatment plans.

Acknowledgements The authors acknowledge and thank the various grants they have received. This study was supported by the National Natural Scientific Foundation of China, Universities Co-funded Project of Key Research and Development Project of Shaanxi Province, the Science and Technology Planning Project of Yulin City, and the Australian Research Council.

Authors contributions Zhenzhen Hu: Conceptualization, Methodology, Validation, Formal analysis, Writing - original draft, Funding acquisition. Jingliang Dong:

Conceptualization, Methodology, Writing - review & editing. Miao Lou: Software, Validation, Investigation, Methodology. Jingbin Zhang: Datacuration, Software, Visualization, Supervision. Ruiping Ma: Project administration, Validation, Data curation. Yusheng Wang: Datacuration, Visualization, Supervision. Minjie Gong: Supervision, Visualization, Methodology. Botao Wang: Project administration, Supervision, Validation. Zhenbo Tong: Software, Validation, Methodology. Hongxian Ren: Software, Supervision, Methodology. Guoxi Zheng: Conceptualization, Methodology, Validation, Formal analysis, Writing - review & editing, Funding acquisition. Ya Zhang: Conceptualization, Methodology, Validation, Formal analysis, Writing - review & editing, Funding acquisition.

Funding This study was supported by the National Natural Scientific Foundation of China (grant number 82000960); Universities Co-funded Project of Key Research and Development Project of Shaanxi Province (grant number 2020GXLH-Y-017); the Science and Technology Planning Project of Yulin City (grant number CXY-2020-047); and the Australian Research Council (grant number DE210101549).

Declarations

Conflict of interest The authors declare that they have no conflict of interest.

References

Acar M, Kankilic ES, Koksal AO, Yilmaz AA, Kocaoz D (2014) Method of the diagnosis of adenoid hypertrophy

for physicians: Adenoid-nasopharynx ratio. J Craniofac Surg 25(5):e438-440. https://doi.org/10.1097/SCS.0000000000000952

Adedeji TO, Amusa YB, Aremu AA (2016) Correlation between adenoidal nasopharyngeal ratio and symptoms of enlarged adenoids in children with adenoidal hypertrophy. Afr J Paediatr Surg 13 (1):14-19. https://doi.org/10.4103/0189-6725.181701

Bahmanzadeh H, Abouali O, Faramarzi M, Ahmadi G (2015) Numerical simulation of airflow and micro-particle deposition in human nasal airway pre- and post-virtual sphenoidotomy surgery. Comput Biol Med 61:8-18. https://doi.org/10.1016/j.compbiomed.2015.03.015

Beni HM, Hassani K, Khorramymehr S (2019) Study of the sneezing effects on the real human upper airway using fluid-structure interaction method. J Braz Soc Mech Sci 41:181. https://doi.org/10.1007/s40430-019-1677-z

Beni HM, Mortazavi H, Islam MS (2022) Biomedical and biophysical limits to mathematical modeling of pulmonary system mechanics: A scoping review on aerosol and drug delivery. Biomech Model Mechanobiol 21(1):79-87. https://doi.org/10.1007/s 10237-021-01531-8

Beni HM, Mortazavi H, Tashvighi E, Islam MS (2022) Investigation of the Upper Respiratory Tract of a Male Smoker with Laryngeal Cancer by Inhaling Air Associated with Various Physical Activity Levels. Atmosphere 13(5):717. https://doi.org/10.3390/atmos13050717

Bitar MA, Birjawi G, Youssef M, Fuleihan N (2009) How frequent is adenoid obstruction? Impact on the diagnostic approach. Pediatr Int 51(4):478-483. https://doi.org/10.1111/j.1442-200X. 2008. 02787.x

Brambilla I, Pusateri A, Pagella F et al (2014) Adenoids in children: Advances in immunology, diagnosis, and surgery. Clin Anat 27(3):346-352. https://doi.org/10.1002/ca.22373

Dong J, Shang Y, Inthavong K, Chan HK, Tu J (2017) Numerical comparison of nasal aerosol administration systems for efficient Nose-to-Brain drug delivery. Pharm Res 35(1):5. https://doi. org/10.1007/s11095-017-2280-6

399 Dong J, Shang Y, Inthavong K, Chan HK, Tu J (2018) Partitioning of dispersed nanoparticles in a realistic nasal
400 passage for targeted drug delivery. Int J Pharmaceut 543(1/2):83-95. https://doi.org/10.1016/j.ijpharm.
401 2018.03.046
402 Dong J, Sun Q, Shang Y, Zhang Y, Tian L, Tu J (2022) Numerical comparison of inspiratory airflow patterns in
403 human nasal cavities with distinct age differences. Int J Numer Method Biomed Eng 38(3):e3565.
404 https://doi.org/10.1002/cnm.3565
405 Doorly DJ, Taylor DJ, Schroter RC (2008) Mechanics of airflow in the human nasal airways. Resp Physiol Neurobi
406 163(1-3):100-110. https://doi.org/10.1016/j.resp. 2008. 07.027
407 Duan H, Xia L, He W, Lin Y, Lu Z, Lan Q (2019) Accuracy of lateral cephalogram for diagnosis of adenoid
408 hypertrophy and posterior upper airway obstruction: A meta-analysis. Int J Pediatr Otorhinolaryngol 119:1-9.
409 https://doi.org/10.1016/j.ijporl.2019.01.011
410 Elwany S (1987) The adenoidal-nasopharyngeal ratio (AN ratio). Its validity in selecting children for adenoid-
411 ectomy. J Laryngol Otol 101(6):569-573. https://doi.org/10.1017/s0022215100102269
412 Feng X, Chen Y, Cai W, Lie SA, Hellen-Halme K, Shi XQ (2021) Aerodynamic characteristics in upper airways
413 among orthodontic patients and its association with adenoid nasopharyngeal ratios in lateral cephalograms.
414 Bmc Med Imaging 21(1):127. https://doi.org/10.1186/s12880-021-00659-4
415 Feng X, Li G, Qu Z, Liu L, Nasstrom K, Shi XQ (2015) Comparative analysis of upper airway volume with
416 lateral cephalograms and cone‐beam computed tomography. Am J Orthod Dentofacial Orthop 147(2):197-
417 204. https://doi.org/10.1016/j.ajodo.2014.10.025
418 Fujioka M, Young LW, Girdany BR (1979) Radiographic evaluation of adenoidal size in children: Adenoidal-
419 nasopharyngeal ratio. AJR Am J Roentgenol 133(3):401-404. https://doi.org/10.2214 /ajr.133.3.401
420 Garcia G, Rhee JS, Senior BA, Kimbell JS (2010) Septal deviation and nasal resistance: An investigation using

virtual surgery and computational fluid dynamics. Am J Rhinol Allergy 24(1):46-53. https://doi.org/10.2500/ajra.2010.24.3428

Ge QJ, Inthavong K, Tu JY (2012) Local deposition fractions of ultrafine particles in a human nasal-sinus cavity CFD model. Inhal Toxicol 24(8):492-505. https://doi.org/10.3109/08958 378.2012.694494

Hofmann W (1982) Mathematical model for the postnatal growth of the human lung. Respir Physiol 49(1):115-129. https://doi.org/10.1016/0034-5687(82)90106-2

Hood CM, Schroter RC, Doorly DJ, Blenke EJSM, Tolley NS (2009) Computational modeling of flow and gas exchange in models of the human maxillary sinus. J Appl Physiol 107(4):1195-1203. https://doi.org/10.1152/japplphysiol.91615.2008

Horschler I, Meinke M, Schroder W (2003) Numerical simulation of the flow field in a model of the nasal cavity. Comput Fluids 32(1):39-45. https://doi.org/10.1016/S0045-7930(01)00097-4

Kindermann CA, Roithmann R, Lubianca NJ (2008) Sensitivity and specificity of nasal flexible fiberoptic endoscopy in the diagnosis of adenoid hypertrophy in children. Int J Pediatr Otorhinolaryngol 72(1):63-67. https://doi.org/10.1016/j.ijporl.2007.09.013

Kubba H, Bingham BJ (2001) Endoscopy in the assessment of children with nasal obstruction. J Laryngol Otol 115(5):380-384. https://doi.org/10.1258/0022215011907929

Lee KB, Jeon YS, Chung SK, Kim SK (2016) Effects of partial middle turbinectomy with varying resection volume and location on nasal functions and airflow characteristics by CFD. Comput Biol Med 77:214-221. https://doi.org/10.1016/j.compbiomed.2016.08.014

Lertsburapa K, Jr. Schroeder JW, Sullivan C (2010) Assessment of adenoid size: A comparison of lateral radiographic measurements, radiologist assessment, and nasal endoscopy. Int J Pediatr Otorhi 74(11):1281-1285. https://doi.org/10.1016/j.ijporl.2010.08.005

Li L, Han D, Zhang L, Li Y, Zang H, Wang T, Liu Y (2016) Impact of nasal septal perforations of varying sizes and locations on the warming function of the nasal cavity: A computational fluid-dynamics analysis of 5 cases. Ear Nose Throat J 95(9):E9-14.https://doi.org/10.1177/01455613160 9500906

Lou M, Zhang L, Zhang J, Ma R, Gong M, Hu Z, Wang S, Zhang Y, Zheng G (2021) Numerical simulation of nasal airflow aerodynamics, and warming and humidification in models of clival chordoma pre and Post-Endoscopic endonasal surgery. Resp Physiol Neurobi 291. https://doi.org/ 10.1016/j.resp.2021.103693

Luo H, Sin S, McDonough JM, Isasi CR, Arens R, Wootton DM (2014) Computational fluid dynamics endpoints for assessment of adenotonsillectomy outcome in obese children with obstructive sleep apnea syndrome. J Biomech 47(10):2498-2503. https://doi.org/10.1016/j.jbio mech.2014.03.023

Major MP, Witmans M, El-Hakim H, Major PW, Flores-Mir C (2014) Agreement between cone-beam computed tomography and nasoendoscopy evaluations of adenoid hypertrophy. Am J Orthod Dentofacial Orthop 146(4):451-459. https://doi.org/10.1016/j.ajodo.2014.06.013

Mihaescu M, Murugappan S, Gutmark E, Donnelly LF, Kalra M (2008) Computational modeling of upper airway before and after adenotonsillectomy for obstructive sleep apnea. Laryngoscope 118(2):360-362. https://doi.org/10.1097/MLG.0b013e31815937c1

Pacheco-Pereira C, Alsufyani NA, Major M, Heo G, Flores-Mir C (2016) Accuracy and reliability of orthodontists using cone-beam computerized tomography for assessment of adenoid hypertrophy. Am J Orthod Dentofac 150(5):782-788. https://doi.org/10.1016/j.ajodo.2016.03.030

Pagella F, De Amici M, Pusateri A et al (2015) Adenoids and clinical symptoms: Epidemiology of a cohort of 795 pediatric patients. Int J Pediatr Otorhinolaryngol 79(12):2137-2141. https://doi.org/10.1016/j.ijporl.2015.09.035

Pereira L, Monyror J, Almeida FT, Almeida FR, Guerra E, Flores-Mir C, Pacheco-Pereira C (2018) Prevalence of

adenoid hypertrophy: A systematic review and meta-analysis. Sleep Med Rev 38:101-112. https://doi.Org/10.1016/j.smrv.2017.06.001

Siu J, Inthavong K, Dong J, Shang Y, Douglas RG (2021) Nasal air conditioning following total inferior turbinectomy compared to inferior turbinoplasty - a computational fluid dynamics study. Clin Biomech (Bristol, Avon) 81:105237. https://doi.org/10.1016/j.clinbiomech.2020.105237

Siu J, Shrestha K, Inthavong K, Shang Y, Douglas R (2020) Particle deposition in the paranasal sinuses following endoscopic sinus surgery. Comput Biol Med 116:103573. https://doi.org/10. 1016/j.compbiomed.2019.103573

Sun Q, Dong J, Zhang Y, Tian L, Tu, J (2022) Numerical study of the effect of nasopharynx airway obstruction on the transport and deposition of nanoparticles in nasal airways. Experimental and Computational Multiphase Flow 4(4): 399-408. https://doi.org/10.1007/s42757-022-0143-9

Ungkanont K, Damrongsak S (2004) Effect of adenoidectomy in children with complex problems of rhinosinusitis and associated diseases. Int J Pediatr Otorhinolaryngol 68(4):447-451. https://doi.org/10. 1016/j.ijporl.2003.11.016

van Cauwenberge PB, Bellussi L, Maw AR, Paradise JL, Solow B (1995) The adenoid as a key factor in upper airway infections. Int J Pediatr Otorhinolaryngol 32:S71-80. https://doi.org/10.101 6/0165-5876(94)01146-o

Wang SM, Inthavong K, Wen J, Tu JY, Xue CL (2009) Comparison of micron- and nanoparticle deposition patterns in a realistic human nasal cavity. Resp Physiol Neurobi 166(3):142-151. https://doi.org/10.1016/j.resp.2009.02.014

Weese J, Lungu A, Peters J, Weber FM, Waechter-Stehle I, Hose DR (2017) CFD- and Bernoulli-based pressure drop estimates: A comparison using patient anatomies from heart and aortic valve segmentation of CT images. Med Phys 44(6):2281-2292. https://doi.org/10.1002/mp.12203

Weir N (1990) Otolaryngology: an illustrated history. Butterworth & Co, London.

Wen J, Inthavong K, Tu J, Wang S (2008) Numerical simulations for detailed airflow dynamics in a human nasal cavity. Respir Physiol Neurobiol 161(2):125-135. https://doi.org/10.1016/j.resp. 2008.01.012

Xi J, Si X, Zhou Y, Kim J, Berlinski A (2014) Growth of nasal and laryngeal airways in children: Implications in breathing and inhaled aerosol dynamics. Respir Care 59(2):263-273. https://doi. org/10.4187/respcare.02568

Xiong G, Zhan J, Zuo K, Li J, Rong L, Xu G (2008) Numerical flow simulation in the post-endoscopic sinus surgery nasal cavity. Med Biol Eng Comput 46(11):1161-1167. https://doi.org/10. 1007/s11517-008-0384-1

Xu C, Sin S, McDonough JM, Udupa JK, Guez A, Arens R, Wootton DM (2006) Computational fluid dynamics modeling of the upper airway of children with obstructive sleep apnea syndrome in steady flow. J Biomech 39(11):2043-2054. https://doi.org/10.1016/j.jbiomech.2005.06.021

Xu X, Wu J, Weng W, Fu M (2020) Investigation of inhalation and exhalation flow pattern in a realistic human upper airway model by PIV experiments and CFD simulations. Biomech Model Mechan 19(5):1679-1695. https://doi.org/10.1007/s10237-020-01299-3

Yan Y, Dong J, Tu J (2023) Comparative modelling of inspiratory airflow and micron particle deposition patterns in monkey and human nasal airways. J Aerosol Sci 167:106099. https://doi.org/https://doi.org/10.1016/j.jaerosci.2022.106099

Zhang Y, Shang Y, Inthavong K, Tong Z, Sun B, Zhu K, Yu A, Zheng G (2019) Computational investigation of dust mite allergens in a realistic human nasal cavity. Inhal Toxicol 31(6):224-235. https://doi.org/10.1080/08958378.2019.1647315

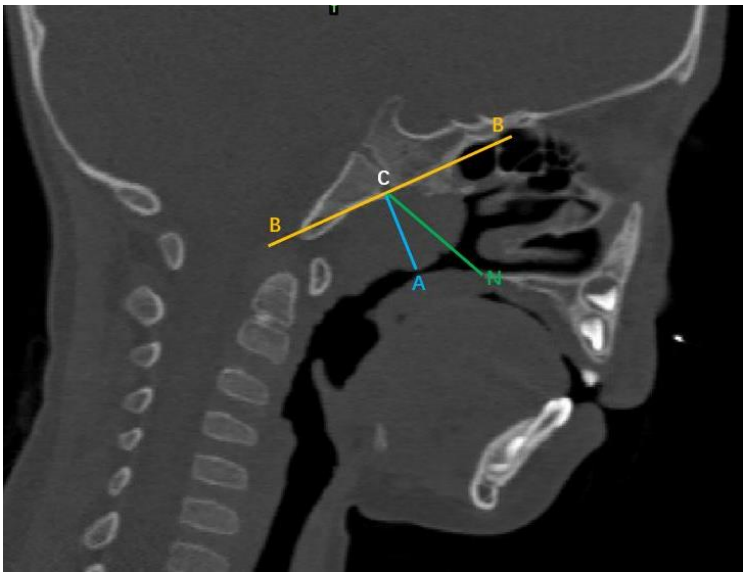

Fig. 1 Method of calculating the adenoidal-nasopharyngeal (AN) ratio based on CT images. BB: Line drawn along the straight part of the anterior margin of the basiocciput; AC: Adenoid thickness (perpendicular distance from the outermost point of convexity of the adenoid shadow to BB); NC: Nasopharyngeal width (distance from the posterior end of the hard palate or the superior edge of the anterior middle area of the soft palate to the anteroinferior edge of the sphenooccipital synchondrosis); AN ratio calculated by dividing AC with NC.

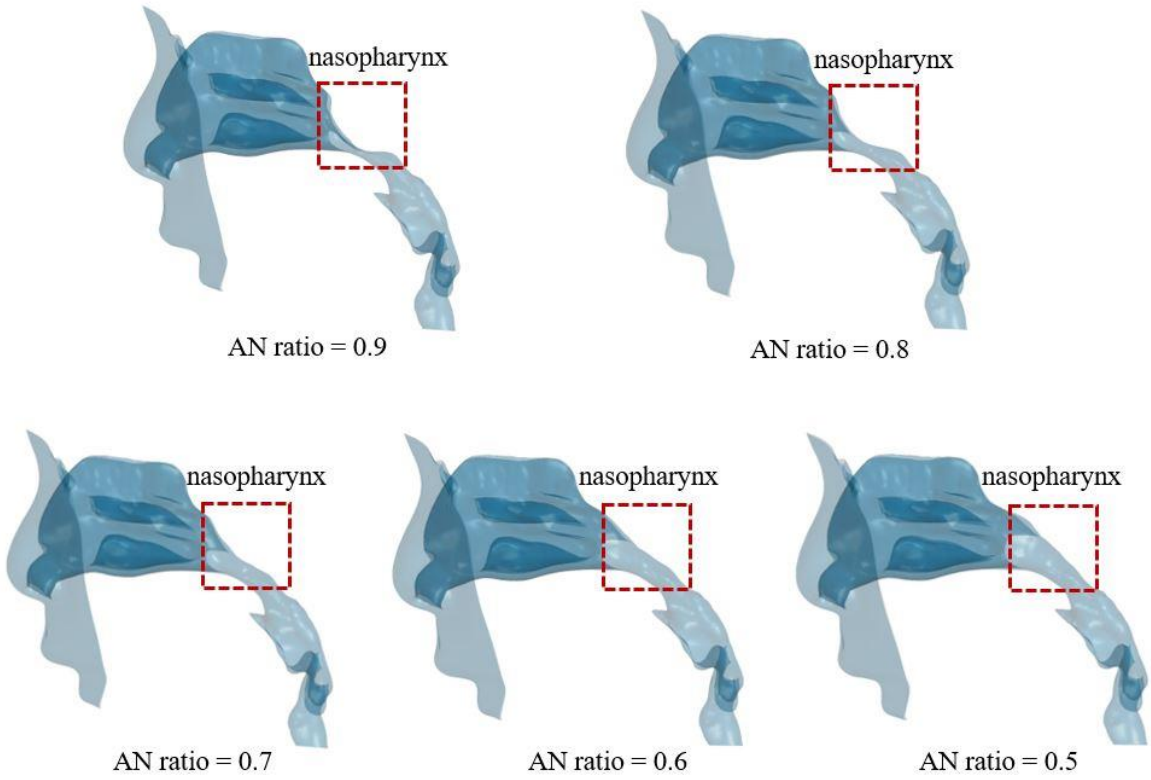

Fig. 2 UA models with AN ratios of 0.9 to 0.5. (UA: upper airway; AN ratio: adenoidal-nasopharyngeal ratio).

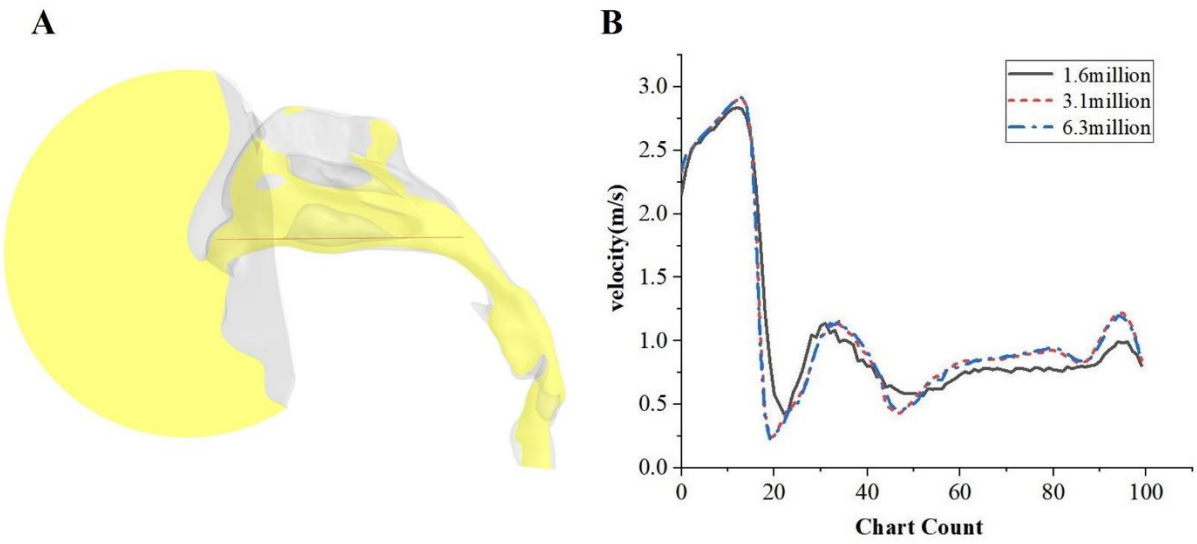

Fig. 3 A shows the position of the line in the nasal cavity. B represents velocity along a representative line in the nasal cavity for a flow rate of Q = 8.7 L/min as predicted by different grids.

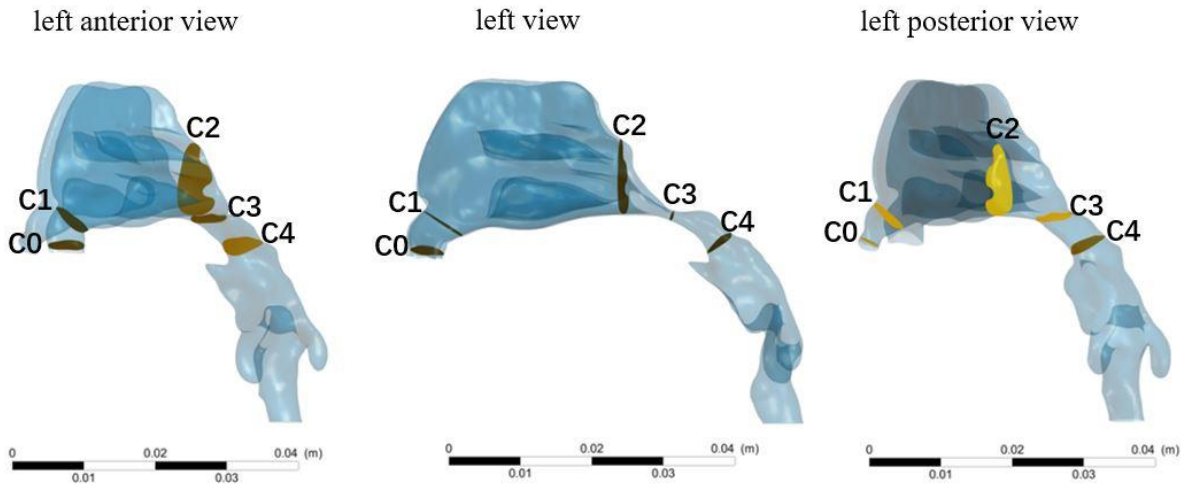

Fig. 4 Typical cross sections within the UA model with an AN ratio of 0.9. (UA: upper airway; AN ratio: adenoidal-nasopharyngeal ratio).

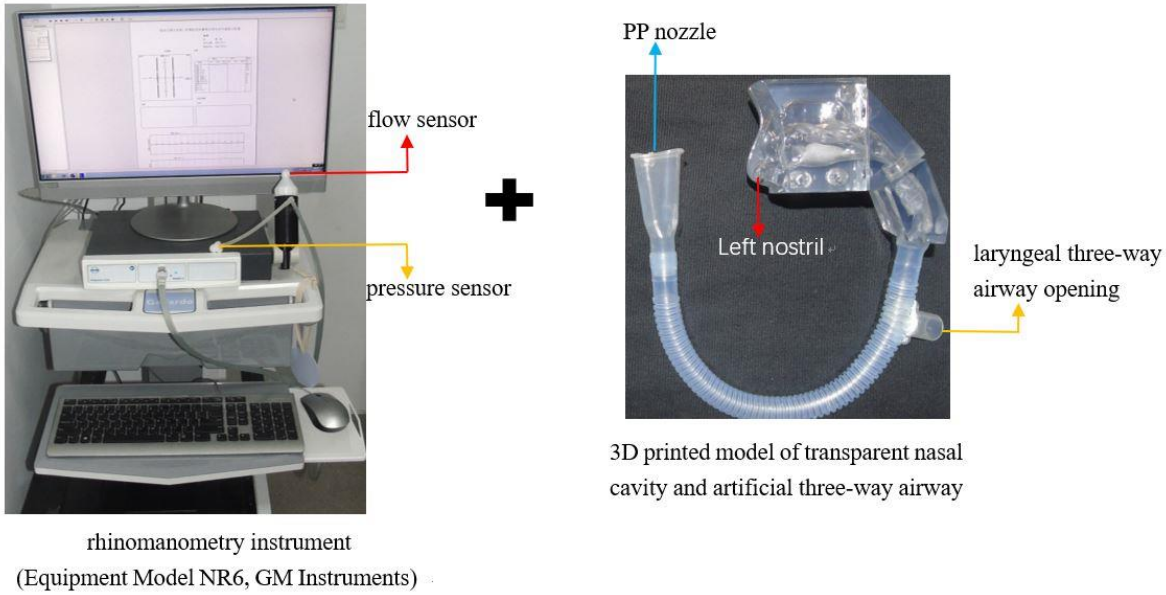

Fig. 5 Schematic diagram of nasal resistance measurement of a 3D printed model. Experimental steps: (1) the flow sensor is placed in the left nostril; (2) the pressure sensor is placed in the opening of the three-way airway at the throat; and (3) the experimenter breathes calmly through the PP nozzle.

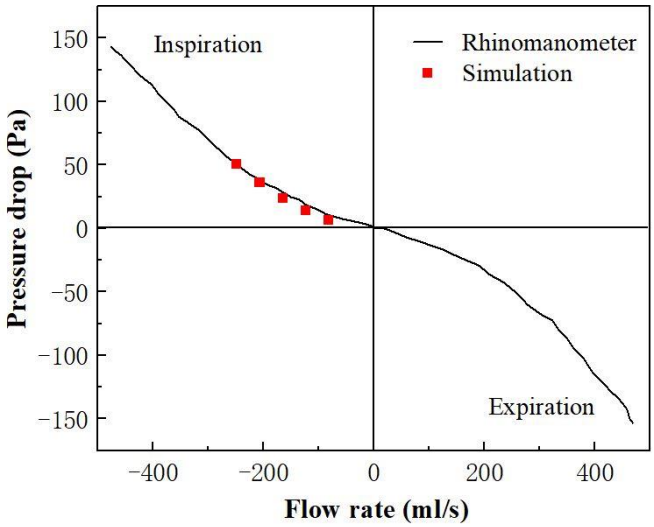

Fig. 6 Comparison of nasal resistances in left nasal cavity numerical red point, and experimental results.

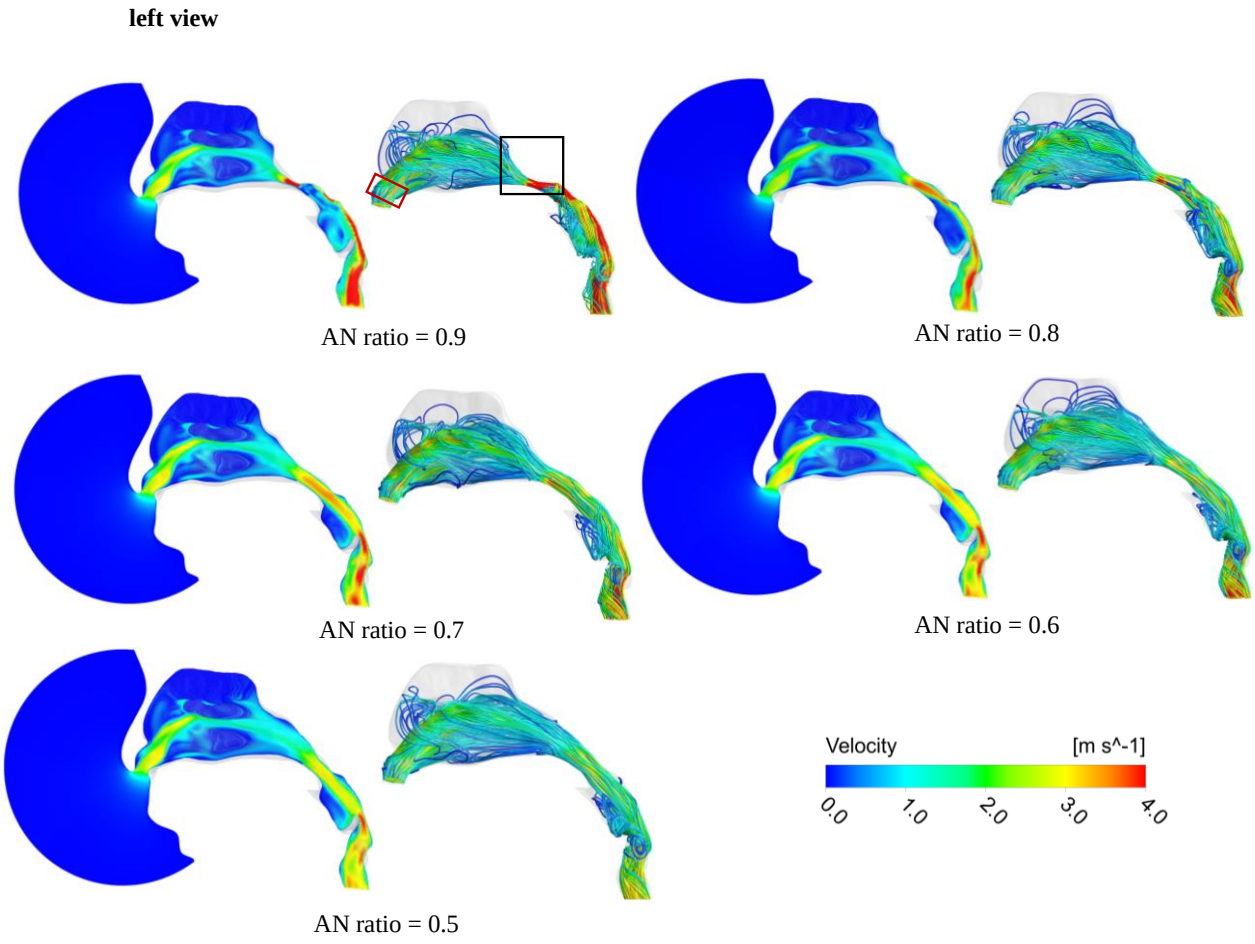

Fig. 7 Streamlines and contours of air velocity in the UA with an AN ratio of 0.9 to 0.5 (the red square is the nasal valve area, and the black square is the nasopharynx). (UA: upper airway; AN ratio: adenoidal-nasopharyngeal ratio).

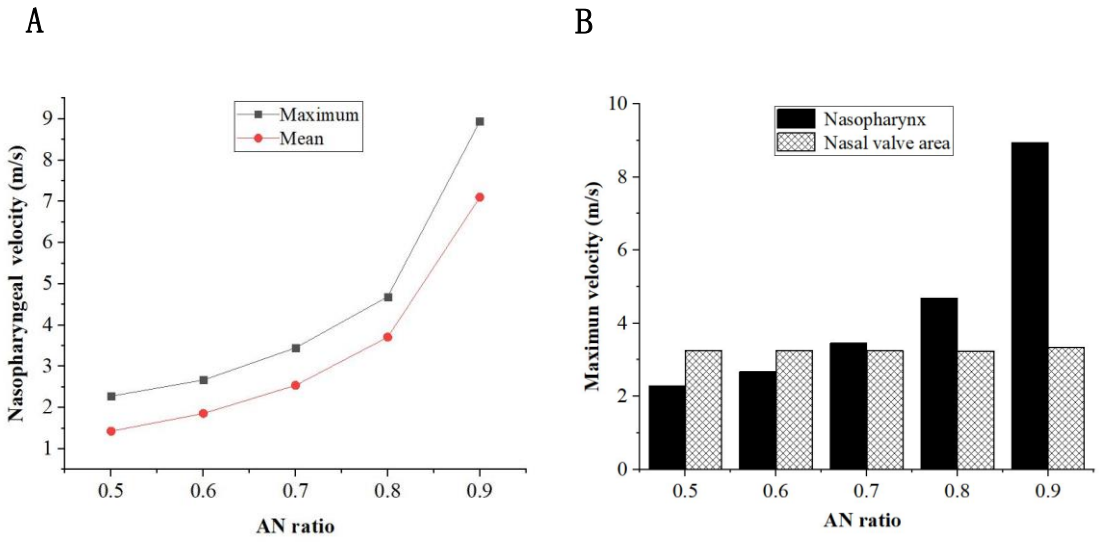

Fig. 8 A displays the maximum and average velocity of the nasopharynx at different AN ratios. B displays the maximum velocity of the nasopharynx and nasal valve area at different AN ratios. (AN ratio: adenoidal-nasopharyngeal ratio).

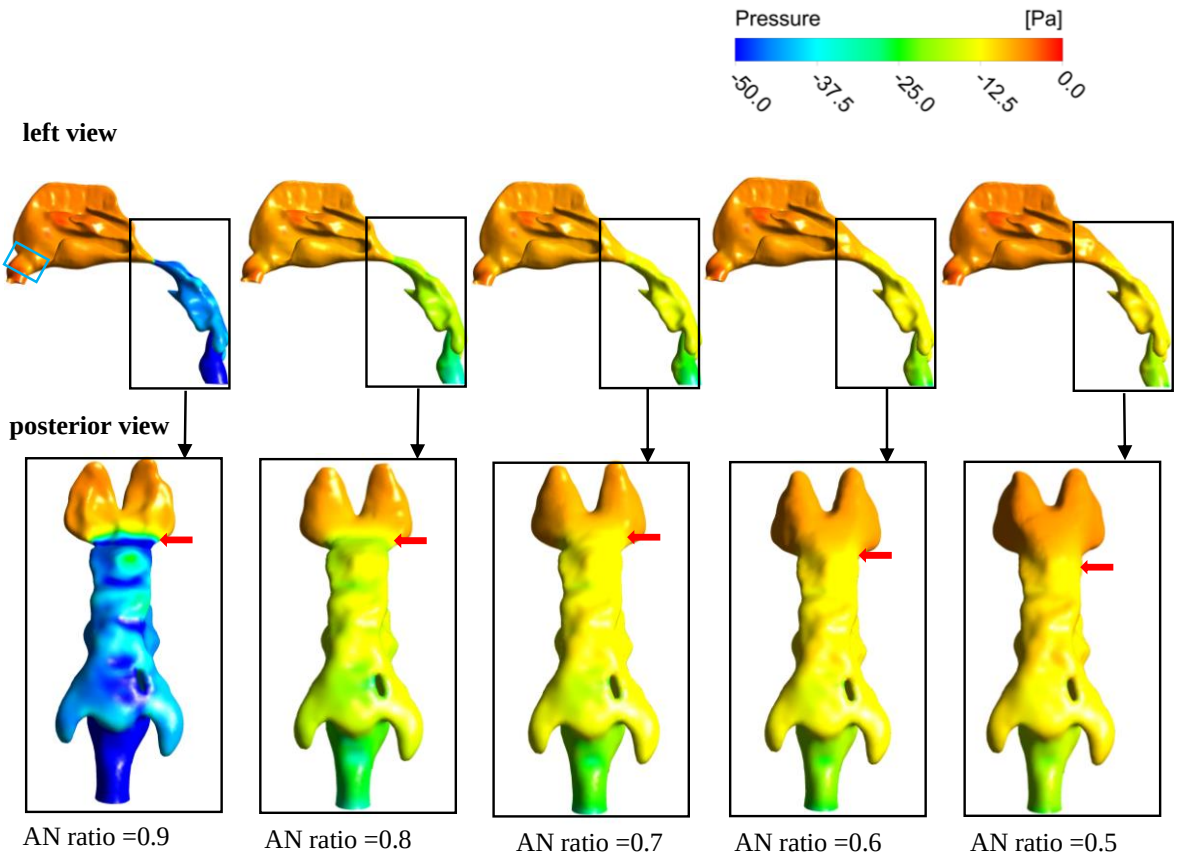

Fig. 9 Pressure contours in the UA with an AN ratio of 0.9 to 0.5 (the blue square is the nasal valve area, the black square is the pharynx, and the red arrows indicate pressure changes in the nasopharynx). (UA: upper airway; AN ratio: adenoidal-nasopharyngeal ratio).

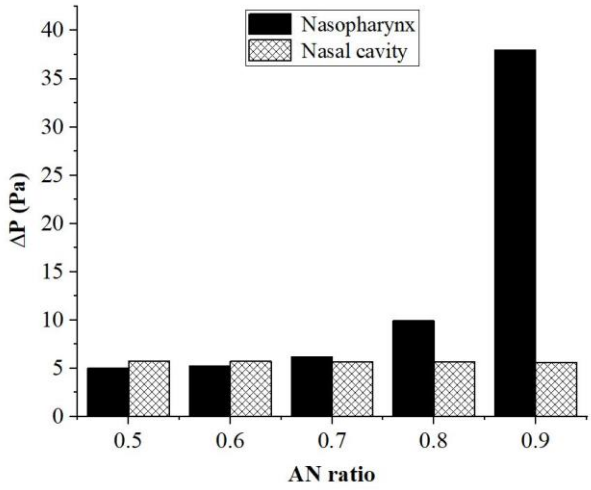

Fig. 10 ΔP in the nasopharynx and nasal cavity at different AN ratios. (△P: pressure drop; AN ratio: adenoidal-nasopharyngeal ratio).

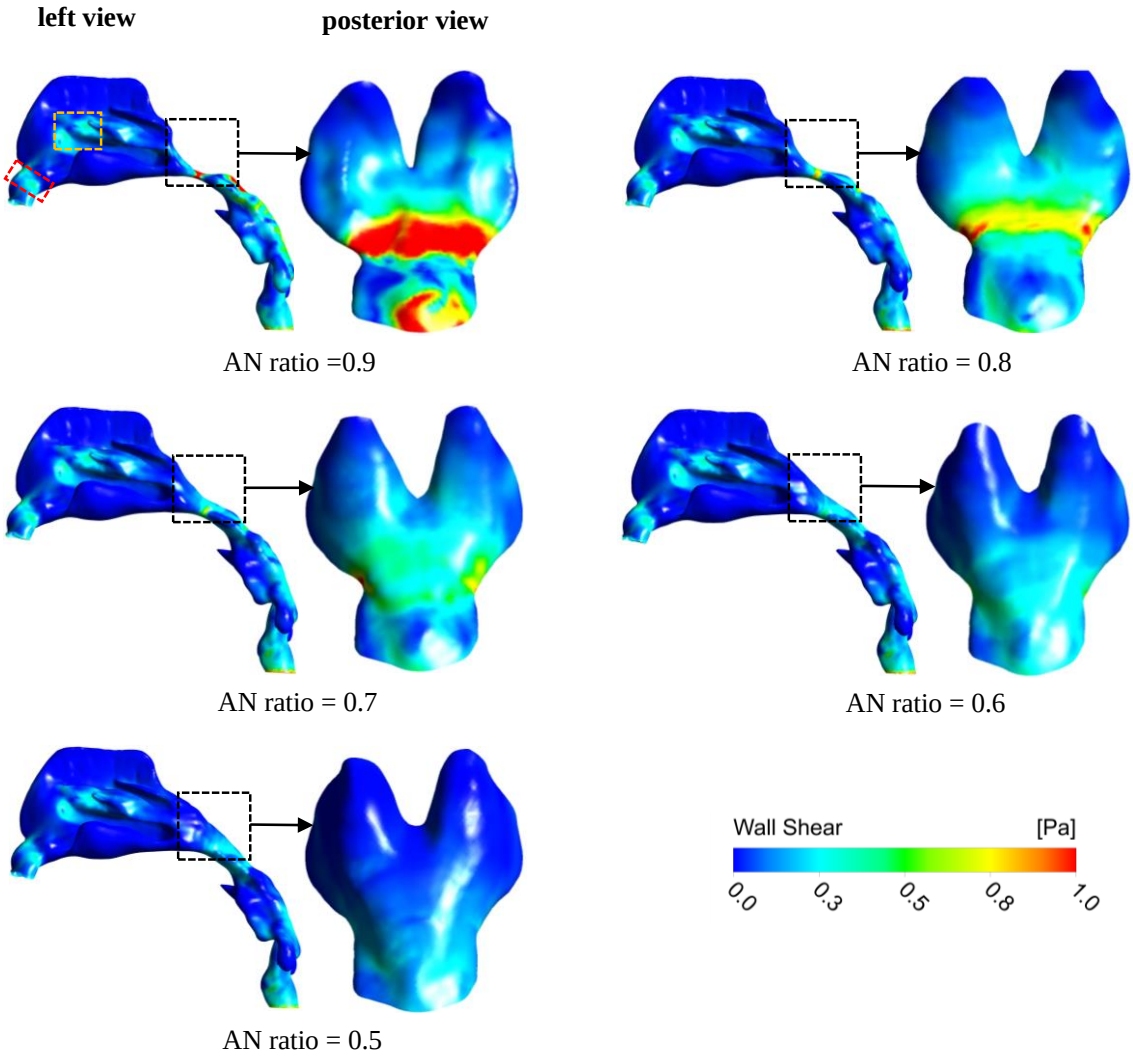

Fig. 11 WSS contours in the UA with an AN ratio of 0.9 to 0.5 (the red square, yellow square and black square represent the WSS in the nasal valve area, the anterior medial area of the middle turbinate and the posterior wall of the nasopharynx, respectively). (WSS: wall shear stress; UA: upper airway; AN ratio: adenoidal-nasopharyngeal ratio).

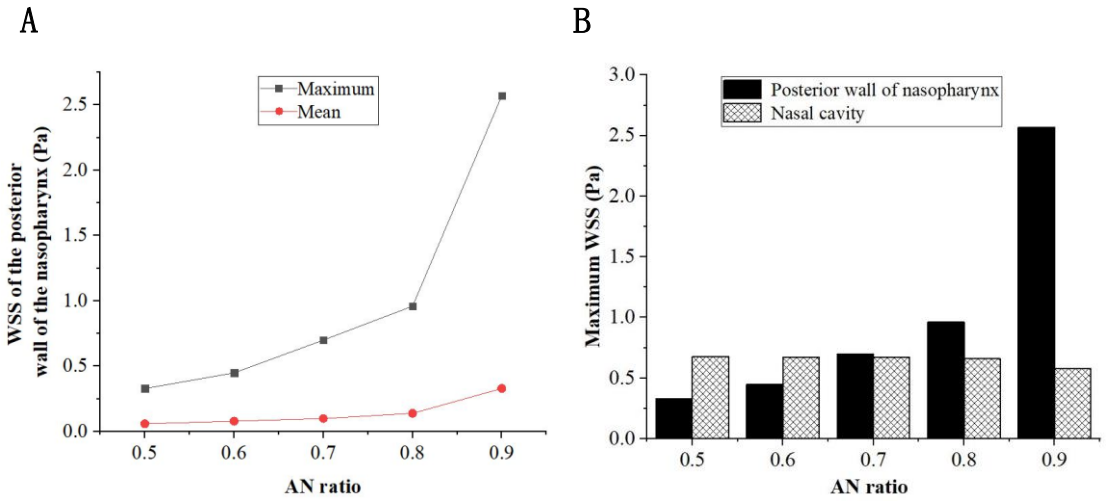

Fig. 12 A displays the maximum and average WSS of the posterior wall of the nasopharynx with different AN ratios. B displays the maximum WSS of the nasal cavity and posterior wall of the nasopharynx at different AN ratios. (WSS: wall shear stress; AN ratio: adenoidal-nasopharyngeal ratio).

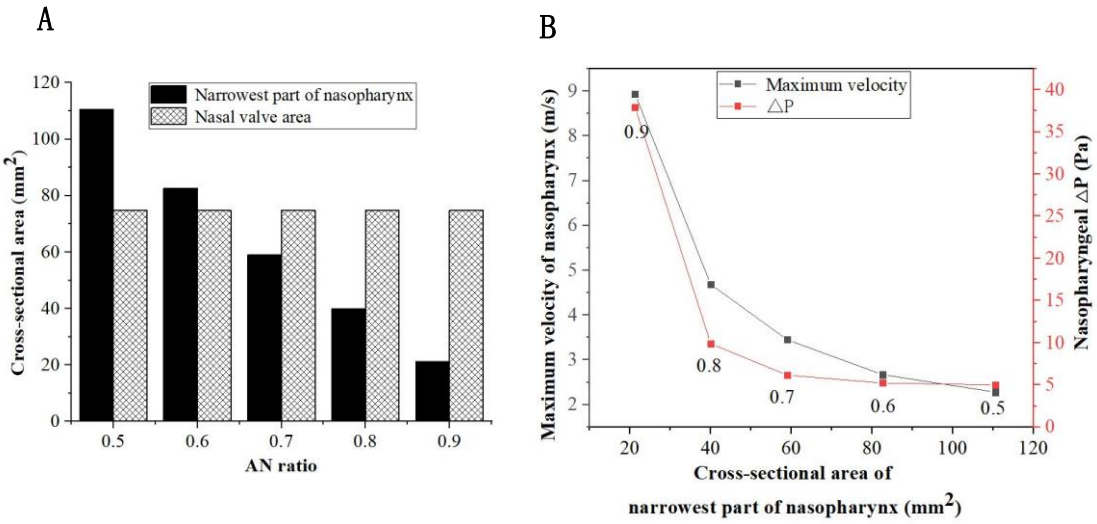

Fig. 13 A displays the cross-sectional area of the nasal valve area and the narrowest part of the nasopharynx at different AN ratios. B displays the relationship of the cross-sectional area of the narrowest part of the nasopharynx with the maximum velocity and ΔP. (AN ratio: adenoidal-nasopharyngeal ratio; ΔP: pressure drop).

Table 1 Key geometric information of the upper airway model

AN ratio of the Model	Grid number	Cross-sectional area of narrowest part of nasopharynx(mm^2)	Nasopharyngeal volume(mm^3)
0.9	5434816	21.21	1380.68
0.8	5506198	39.96	1635.84
0.7	5564851	58.94	1973.34
0.6	5623245	82.59	2439.86
0.5	5690966	110.61	2857.81

AN ratio: adenoidal-nasopharyngeal ratio